supported metal clusters from extended metal surfaces. These effects (and thus opportunities for tuning catalytic properties by choice of the support) are most pronounced for the smallest clusters, and may be negligible for large supported metal particles for which only a small fraction of the metal atoms are bonded to the support.

Purely geometric effects can also distinguish the catalytic activity seen with small metal clusters from that seen with bulk metal or larger supported particles, by limiting the structures that can bond to a very small cluster and subsequently react on it. For example, propylidyne is stable on Ir_4/γ-Al_2O_3 when treated in He or H_2 at temperatures up to 523 K (ref. 8), whereas propylidyne on extended metal surfaces[17,20] decomposes thermally under vacuum at 403–433 K and is largely hydrogenated in the presence of H_2 at room temperature. This qualitative difference in reactivity is attributed to the presence of neighbouring metal centres that facilitate reaction on the extended surfaces, and the lack of such centres on isolated Ir_4 (ref. 8). Thus, propylidyne on Pt(111) undergoes catalytic hydrogenation[15] whereas propylidyne at saturation concentration on Ir_4/γ-Al_2O_3 does not react, rendering the clusters almost inactive for propene hydrogenation (Table 1). □

Received 16 August; accepted 11 December 2001.

1. Collman, J. P., Hegedus, L. S., Norton, J. R. & Finke, R. G. *Principles and Applications of Organotransition Metal Chemistry* 2nd edn (University Science Books, Mill Valley, California, 1987).
2. Stevenson, S. A., Dumesic, J. A., Baker, R. T. K. & Ruckenstein, E. (eds) *Metal-Support Interactions in Catalysis, Sintering, and Redispersion* (van Nostrand Reinhold, New York, 1987).
3. Haller, G. L. & Resasco, D. E. Metal-support interaction: group VIII metals and reducible oxides. *Adv. Catal.* **36,** 173–235 (1989).
4. Yudanov, I. V., Vent, S., Neyman, K., Pacchioni, G. & Rösch, N. Adsorption of Pd atoms and Pd-4 clusters on the MgO(001) surface: a density functional study. *Chem. Phys. Lett.* **275,** 245–252 (1997).
5. Matveev, A. V., Neyman, K., Pacchioni, G. & Rösch, N. Density functional study of M-4 clusters (M = Cu, Ag, Ni, Pd) deposited on the regular MgO(001) surface. *Chem. Phys. Lett.* **299,** 603–612 (1999).
6. Goellner, J. V. *et al.* Ligand-free osmium clusters supported on MgO: a density functional study. *Langmuir* **16,** 2736–2743 (2000).
7. Ferrari, A. M. *et al.* Faujasite-supported Ir_4 clusters: A density functional model study of metal–zeolite interactions. *J. Phys. Chem. B.* **103,** 5311–5319 (1999).
8. Argo, A. M., Goellner, J. F., Phillips, B. L., Panjabi, G. A. & Gates, B. C. Reactivity of site-isolated metal clusters: propylidyne on γ-Al_2O_3-supported Ir_4. *J. Am. Chem. Soc.* **123,** 2275–2283 (2001).
9. McVicker, G. B. *et al.* Effect of sulfur on the performance and on the particle size and location of platinum in Pt/KL hexane aromatization catalyst. *J. Catal.* **139,** 48–61 (1993).
10. Jentoft, R. E., Tsapatsis, M., Davis, M. E. & Gates, B. C. Platinum clusters supported in zeolite LTL: influence of catalyst morphology on performance in *n*-hexane reforming. *J. Catal.* **179,** 565–580 (1998).
11. Xu, Z. *et al.* Size-dependent catalytic activity of supported metal clusters. *Nature* **372,** 346–348 (1994).
12. Gates, B. C. Supported metal clusters: synthesis, structure, and catalysis. *Chem. Rev.* **95,** 511–522 (1995).
13. Argo, A. M. *Influence of Supports, Cluster Structure, and Cluster Composition on Hydrogenation Reactions Catalyzed by Oxide-Supported Metal Clusters.* Thesis, Univ. California at Davis (2001).
14. Odzak, J. F., Argo, A. M., Lai, F. S. & Gates, B. C. A flow through X-ray absorption spectroscopy cell for characterization of powder catalysts in the working state. *Rev. Sci. Instrum.* **72,** 3943–3945 (2001).
15. Cremer, P. S., Su, X., Shen, Y. R. & Somorjai, G. A. Hydrogenation and dehydrogenation of propylene on Pt(111) studied by sum frequency generation from UHV to atmospheric pressure. *J. Phys. Chem.* **100,** 16302–16309 (1996).
16. Cremer, P. S., Su, X., Shen, Y. R. & Somorjai, G. A. Ethylene hydrogenation on Pt(111) monitored in situ at high pressure using sum frequency generation. *J. Am. Chem. Soc.* **118,** 2942–2949 (1996).
17. Shahid, G. & Sheppard, N. Infrared spectra and the structures of the chemisorbed species resulting from the adsorption of propene and propane on a Pt/SiO_2 catalyst. *Spectrochim. Acta. A* **46,** 999–1010 (1990).
18. Newell, H. E., McCoustra, M. R. S., Chesters, M. A. & De La Cruz, C. The thermal chemistry of adsorbed ethyl on the Pt(111) surface: infrared evidence for an ethylidene intermediate in the ethyl to ethylidyne conversion. *J. Chem. Soc. Faraday Trans.* **94,** 3695–3698 (1998).
19. Bent, B. E., Mate, C. M., Crowell, J. E., Koel, B. E. & Somorjai, G. A. Bonding and thermal decomposition of propylene, propadiene, and methylacetylene on the Rh(111) single crystal surface. *J. Phys. Chem.* **91,** 1493–1502 (1987).
20. Chesters, M. A. *et al.* Infrared spectroscopic comparison of the chemisorbed species from ethene, propene, but-1-ene and *cis*- and *trans*-but-2-ene on Pt(111) and on a platinum/silica catalyst. *J. Chem. Soc. Faraday Trans.* **86,** 2757–2763 (1990).
21. Neurock, M. & van Santen, R. A. A first principles analysis of C–H bond formation in ethylene hydrogenation. *J. Phys. Chem. B* **104,** 11127–11145 (2000).

Supplementary Information accompanies the paper on *Nature*'s website (http://www.nature.com).

Acknowledgements

We thank the US National Science Foundation for support and the National Synchrotron Light Source at Brookhaven National Laboratory for beam time.

Competing interests statement

The authors declare that they have no competing financial interests.

Correspondence and requests for materials should be addressed to B.C.G. (email: bcgates@ucdavis.edu).

Towards robust regional estimates of CO_2 sources and sinks using atmospheric transport models

Kevin Robert Gurney*, Rachel M. Law†, A. Scott Denning*, Peter J. Rayner†, David Baker‡, Philippe Bousquet§, Lori Bruhwiler‖, Yu-Han Chen¶, Philippe Ciais§, Songmiao Fan#, Inez Y. Fung☆, Manuel Gloor, Martin Heimann**, Kaz Higuchi††, Jasmin John☆, Takashi Maki‡‡, Shamil Maksyutov§§, Ken Masarie‖, Philippe Peylin§, Michael Prather‖‖, Bernard C. Pak‖‖, James Randerson¶¶, Jorge Sarmiento#, Shoichi Taguchi##, Taro Takahashi☆☆ & Chiu-Wai Yuen****

** Department of Atmospheric Science, Colorado State University, Fort Collins, Colorado 80523, USA*
† CSIRO Atmospheric Research, PMB 1, Aspendale, Victoria 3195, Australia
‡ National Center for Atmospheric Research (NCAR), Boulder, Colorado 80303, USA
§ Laboratoire des Sciences du Climat et de l'Environnement (LSCE), F-91198 Gif-sur-Yvette Cedex, France
‖ Climate Monitoring and Diagnostics Laboratory, National Oceanic and Atmospheric Administration (NOAA), 326 Broadway R/CG1, Boulder, Colorado 80303, USA
¶ Department of Earth, Atmospheric, and Planetary Science, Massachusetts Institute of Technology, Cambridge, Massachusetts 02141, USA
 # AOS Program, Princeton University, Sayre Hall, Forrestal Campus, PO Box CN710, Princeton, New Jersey 08544-0710, USA
☆ Center for Atmospheric Sciences, McCone Hall, University of California, Berkeley, California 94720-4767, USA
*** Max-Planck-Institut fur Biogeochemie, D-07701 Jena, Germany*
†† Meteorological Service of Canada, Environment Canada, Toronto, Ontario M3H 5T4, Canada
‡‡ Quality Assurance Section, Atmospheric Environment Division, Observations Department, Japan Meteorological Agency, 1-3-4 Otemachi, Chiyoda-ku, Tokyo 100-8122, Japan
§§ Institute for Global Change Research, Frontier Research System for Global Change, Yokohama 236-0001, Japan
‖‖ Earth System Science, University of California, Irvine, California 92697-3100, USA
¶¶ Divisions of Engineering and Applied Science and Geological and Planetary Sciences, California Institute of Technology, Mail Stop 100-23, Pasadena, California 91125, USA
National Institute of Advanced Industrial Science and Technology, 16-1 Onogawa Tsukuba, Ibaraki 305-8569, Japan
☆☆ Lamont-Doherty Earth Observatory of Columbia University, Palisades, New York 10964, USA

Information about regional carbon sources and sinks can be derived from variations in observed atmospheric CO_2 concentrations via inverse modelling with atmospheric tracer transport models. A consensus has not yet been reached regarding the size and distribution of regional carbon fluxes obtained using this approach, partly owing to the use of several different atmospheric transport models[1–9]. Here we report estimates of surface–atmosphere CO_2 fluxes from an intercomparison of atmospheric CO_2 inversion models (the TransCom 3 project), which includes 16 transport models and model variants. We find an uptake of CO_2

© 2002 Macmillan Magazines Ltd

in the southern extratropical ocean less than that estimated from ocean measurements, a result that is not sensitive to transport models or methodological approaches. We also find a northern land carbon sink that is distributed relatively evenly among the continents of the Northern Hemisphere, but these results show some sensitivity to transport differences among models, especially in how they respond to seasonal terrestrial exchange of CO_2. Overall, carbon fluxes integrated over latitudinal zones are strongly constrained by observations in the middle to high latitudes. Further significant constraints to our understanding of regional carbon fluxes will therefore require improvements in transport models and expansion of the CO_2 observation network within the tropics.

We estimate annual average fluxes for the 1992–96 period using each transport model and a common inversion set-up (see Methods). Methodological choices for this 'control' inversion have been selected on the basis of knowledge gained from a wide range of sensitivity tests (to be reported elsewhere). Performing the inversion with multiple transport models gives mean estimated fluxes that are relatively insensitive to reasonable variations in the set-up—and estimated uncertainties that represent a more complete estimate of the true uncertainty. The maximum number of regions in our inversion and the spatial distributions of fluxes within each region are fixed, precluding sensitivity tests of these inversion components.

Figure 1 shows the mean flux estimates (left-hand cross in each box) and two uncertainty measures for the control inversion. The first uncertainty measure is the mean of the individual model flux uncertainties (circles) which we designate the 'within-model' uncertainty. For any region, this estimated flux uncertainty must be smaller than the prior flux uncertainty (outer bounds of the boxes). The magnitude of the decrease indicates the degree to which the final flux estimate is constrained by the measurements. Figure 1 shows that the northern land regions and Australia are better constrained by the measurements than are the remaining land regions. The Southern Ocean region is well constrained by the atmospheric measurements, in part because it is treated as a single large region. The Atlantic regions are constrained more by their prior flux uncertainties, which are relatively small due to better coverage of ocean measurements in these regions.

The second uncertainty measure is the standard deviation of the flux estimates over the ensemble of models (error bars in Fig. 1). We call this the 'between-model' uncertainty. This measure indicates the degree to which transport model differences contribute to the range of flux estimates. Large between-model uncertainties are found for northern Africa, tropical America, temperate Asia and boreal Asia (all greater than 0.5 Gt C yr^{-1}).

For most regions, the between-model uncertainties are of similar or smaller magnitude than the within-model uncertainties. This suggests that the choice of transport model is not the critical determinant of the inferred fluxes. Comparing the uncertainties between regions indicates where the inversion would benefit most from new observations, and where model improvements are most needed. In this particular inversion, new measurements would be most useful over tropical continents and in the South America and South Atlantic regions, while the focus for resolving transport differences would be the northern and tropical land regions.

Regarding the model mean flux estimates, two results deserve attention. First, we find consistency between the ocean fluxes predicted in this study and those based on a global database[10] of CO_2 partial pressure (p_{CO_2}), except in the Southern Ocean where the carbon uptake estimated here is roughly half that based on the p_{CO_2} database. This shift in uptake from south to north is required to match simultaneously large-scale concentration gradients (Fig. 2) and growth rates.

The mismatch between atmospheric and ocean estimates of the Southern Ocean fluxes had been noted a decade ago[11]. Our sensitivity tests find that the near-uniformity of observed concentration in the Southern Hemisphere and the small uncertainty associated with those measurements make this result robust to the choice of observing network, prior flux estimates, global ocean constraint, and transport (see Fig. 2 in Supplementary Information). The discrepancy also cannot be explained by a systematic bias in transport models, as the north–south transport has been investigated in a recent intercomparison[12] where successful simulations of the observed meridional gradient in SF_6 suggested reasonable veracity in gross interhemispheric transport.

One possible reconciliation between the p_{CO_2} database and the inverse result presented here is suggested by recent ocean measurements taken during January and August 2000 in the Indian

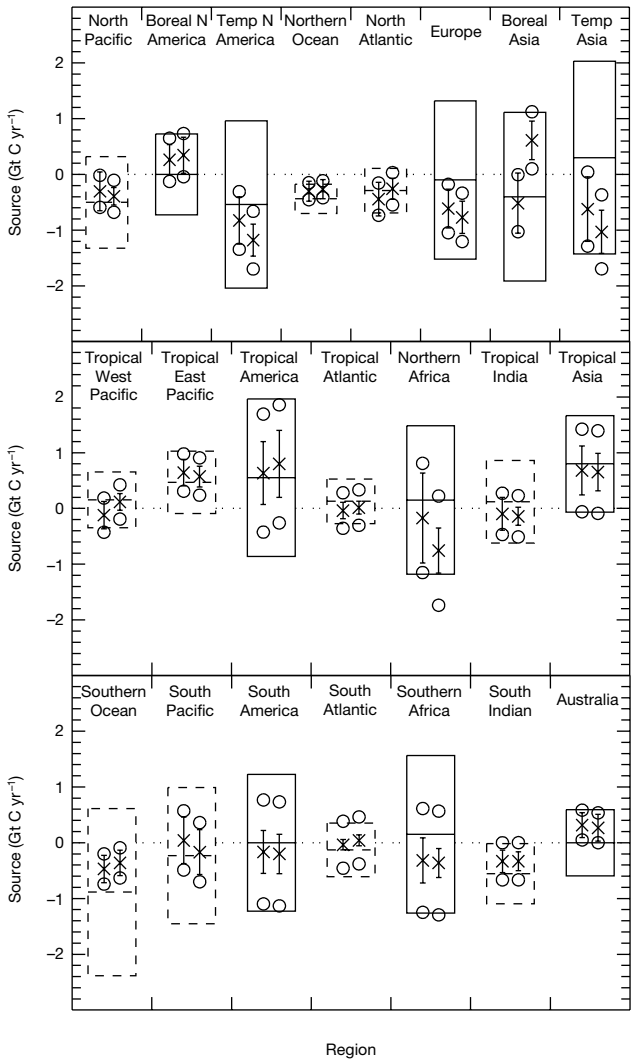

Figure 1 Mean estimated sources and uncertainties for two inversions. Left-hand symbols in each box are for the control inversion, right-hand symbols are for an inversion without the background seasonal biosphere flux. Mean estimated fluxes are shown by crosses, and include all background fluxes except fossil fuel. Positive values indicate a source to the atmosphere. The prior flux estimates and their uncertainties are indicated by the boxes (solid for land, dashed for ocean); the central horizontal bar indicates the prior flux estimate, and the top and bottom of the box give the prior flux uncertainty range. The mean estimated uncertainty across all models (the 'within-model' uncertainty) is indicated by the circles. The standard deviation of the models' estimated fluxes (the 'between-model' uncertainty) is indicated by the 'error bars'. Regions are shown in their approximate north–south and east–west relationship.

© 2002 Macmillan Magazines Ltd

Antarctic sector of the Southern Ocean[13]. The p_{CO_2} values south of 50° S showed seasonal variations that require CO_2 uptake in summer and emission in winter. If the seasonality exhibited in this campaign is true for other parts of the Southern Ocean, this would result in a reduction of the Southern Ocean flux uptake in the database, which is currently determined predominantly by summer measurements. This seasonality-driven explanation is also consistent with forthcoming results from the second stage of the TransCom 3 comparison in which we estimate seasonal cycles (K.R.G. *et al.*, manuscript in preparation).

Second, we find carbon uptake over the continents of the Northern Hemisphere to be distributed relatively evenly across North America, Europe and Asia, in contrast to the distribution found in an earlier, widely cited inverse study[2]. We find a temperate North American sink approximately 60% of that found in the earlier study, a small boreal North American source rather than small uptake, and a large sink for Eurasia rather than an approximately neutral flux. Estimated uncertainties are moderate (0.4–0.7 Gt C yr^{-1}), indicating that regional partitioning remains difficult, but the flux differences between the two studies lie at the edge of (or outside) the uncertainty ranges.

Although previous studies have challenged the possibility of a large North American sink[3–7], little systematic exploration has been performed as to how such a result was achieved. The differences are not due to the choice of transport model, because the two models used in the earlier study are included here and lie in the middle of our range. Extensive sensitivity tests (see Tables 3 and 4 in Supplementary Information) indicate that the Eurasian flux estimate is very sensitive to the pattern of background fluxes used in the inversion, especially that representing the seasonal terrestrial biosphere. The difference in North American uptake results from a combination of methodological choices as well as differences in time period and observational stations used.

There are three methodological differences that together appear to be critical. First, recent work[14] suggests that the larger the region size in an inversion, the greater the potential for producing biased flux estimates. Second, the potential bias can be reduced by increasing the data uncertainty for sites in regions with spatially heterogeneous fluxes. The earlier study[2] inverted for larger regions than used here, and used relatively small (0.6 p.p.m.), spatially invariant uncertainties compared to the generally larger, variable uncertainties used in this study. The third factor is the uncertainty assigned to prior estimates of ocean fluxes, which were zero in the earlier study. Thus the flux adjustment required to match the atmospheric data was applied only to land regions. Together these three factors suggest that the earlier study had greater potential for biased and more sensitive flux estimates than the control results presented here.

Although transport uncertainties do not overwhelm our flux estimates, one factor appears to be responsible for a significant portion of the model spread; the 'rectifier' produced by the covariance between the seasonal biospheric background flux and atmospheric transport[15]. The effect of the rectifier can be seen by performing the inversion without the background biospheric fluxes (Fig. 1, right-hand symbols within each box). The between-model uncertainty is reduced for almost all regions, and in some regions there are substantial changes to the estimated fluxes. An increase of 1.1 Gt C yr^{-1} in boreal Asia changes it from a moderate sink to a moderate source, because rectification produces the strongest concentrations downwind of this region in many of the models. Sink strengths increase by 0.35–0.55 Gt C yr^{-1} for temperate North America, temperate Asia and northern Africa, to maintain the required global source. Measurements indicating the strength of the covariance effect in nature are needed to assess this aspect of model transport.

One way to reduce the large uncertainties in our full calculation is to aggregate our regions after performing the inversion. Figure 3 shows the flux estimates for the land and ocean separately in the southern extratropics, tropics, northern extratropics and for the

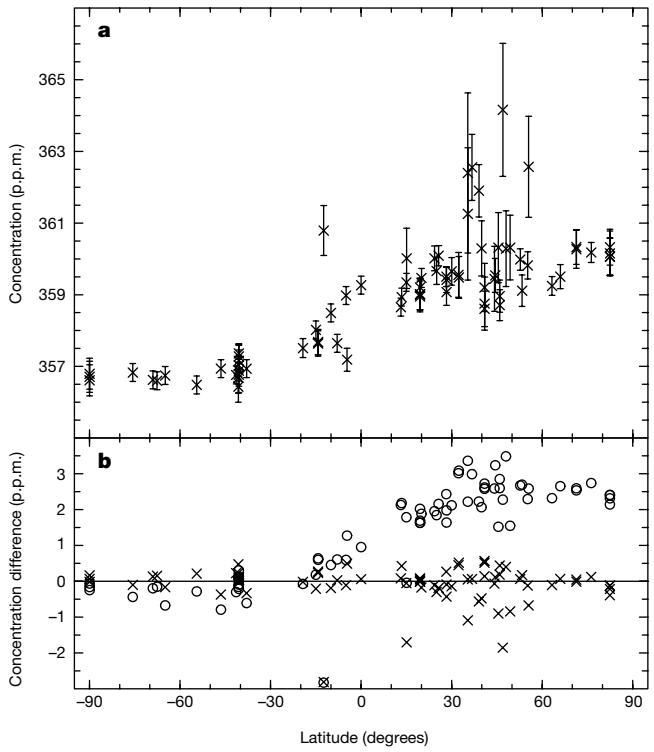

Figure 2 CO_2 concentrations input to, and as fitted by, the inversion. **a**, Meridional gradient of observational CO_2 values and the uncertainty assigned to them in the inversion. **b**, Model mean concentrations for the sum of the three background fluxes minus the observational CO_2 values (circles) and the model mean concentrations after inverting for regional fluxes minus the observational CO_2 values (crosses). Concentrations are 1992 to 1996 means. Note that the adjustment to the background fluxes requires additional uptake in the Northern Hemisphere and lessened uptake in the Southern Hemisphere for all models.

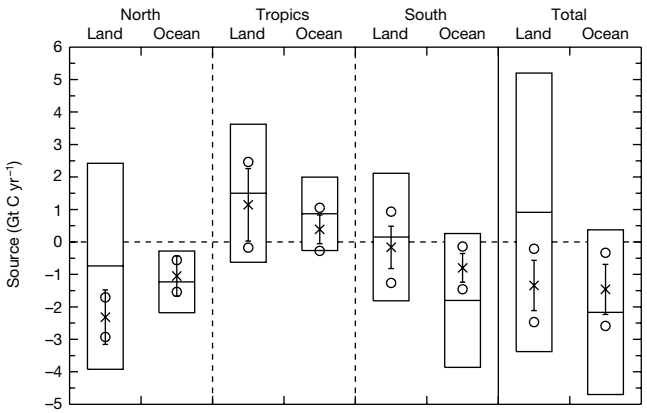

Figure 3 Mean sources and uncertainties for six aggregated regions and global land and ocean. Symbols as in Fig. 1 with the regional aggregation as follows: northern land (boreal North America, temperate North America, Europe, temperate Asia, boreal Asia), tropical land (tropical America, northern Africa, tropical Asia), southern land (South America, southern Africa, Australia), northern ocean (North Pacific, Northern Ocean, North Atlantic) tropical ocean (tropical west Pacific, tropical east Pacific, tropical Atlantic, tropical Indian), southern ocean (Southern Ocean, South Atlantic, South Indian).

© 2002 Macmillan Magazines Ltd

globe as a whole. Within-model uncertainties are reduced relative to simply summing from constituent regions, because much of the uncertainty occurs at the scale of the original regions. There is also a reduction in the between-model uncertainty for this aggregation, as some of the model spread involves details of regional transport. At this larger scale, the decrease in the sink in the Southern Ocean and the enhanced sinks over the Northern Hemisphere appear more significant. The uncertainty on the tropical land region is large; lack of atmospheric data in this region means that inversion methods cannot reliably comment on the extent to which sources due to tropical land-use change are balanced by enhanced growth.

This first stage of the TransCom 3 intercomparison has explored many aspects of annual mean inversions more comprehensively than previous work. By incorporating a range of transport models, the fluxes and their uncertainties represent progress towards more robust inverse estimates of regional carbon exchange. Carbon exchange with the ocean is well constrained in this study and, in the case of the Southern Ocean region, is different from fluxes suggested by p_{CO_2} measurements. This result is consistent across the 16 transport models used here, and is insensitive to many aspects of the inversion set-up. Flux estimates in the northern extratropical land regions are reasonably robust as zonal means, but are difficult to distinguish in the longitudinal direction, and can be biased owing to key methodological aspects of the inversion construction. Seasonal exchange with the terrestrial biosphere is responsible for much of the model spread over these regions. Realistic characterization of this aspect of model transport is essential if this uncertainty is to be reduced in the future.

Flux estimates in the tropical land regions remain very uncertain, owing to few CO_2 observations and the limited influence of extratropical observations on the tropical land flux estimates. New observations that can be represented by global-scale transport models are needed in these regions. Future TransCom analysis will focus on the effect of transport model differences on flux estimates at seasonal and interannual timescales. □

Methods

We use a bayesian synthesis inversion formalism[16] that specifies prior estimates of both the fluxes and their uncertainty, and optimizes with respect to atmospheric observations that are also uncertain. We estimate fluxes for 11 land and 11 ocean regions (see Supplementary Information) as differences from 'background' fluxes that are run separately through each transport model and represent fossil-fuel emissions[17,18], seasonally varying air–sea gas exchange[10] and an annually balanced, seasonally varying flux due to terrestrial photosynthesis and respiration[19]. The use of seasonally varying background fluxes allows the annual mean inversion to include contributions to annual mean concentrations due to the covariance of atmospheric transport and seasonal fluxes.

We invert 5-year mean measurements for 1992–96 at 76 sites taken from the GLOBALVIEW-2000 data set[20] (see Supplementary Information). GLOBALVIEW is a data product that interpolates CO_2 measurements to a common time interval. Gaps in the data are filled by extrapolation from marine boundary layer measurements. We have chosen to use sites where the extrapolated data accounts for less than 30% of the 1992–96 period. The measurements are weighted inversely by the degree to which the predicted concentrations are required by the inverse process to match the observations, which we refer to as 'data uncertainty'. In addition to measurement precision, this uncertainty incorporates the inability of coarse-grid models to adequately represent discrete measurements. The relative uncertainty of one site to another was based on the mean residual standard deviations for 1992–96 from GLOBALVIEW. The absolute magnitudes were chosen to produce a mean square normalized residual out of the inversion of about 1.0, ensuring that the estimated fluxes were optimized to the data only to an appropriate level commensurate with our ability to model them. A minimum uncertainty was also specified. This gave uncertainties ranging from 0.25 p.p.m. for remote, 'clean air' sites to 2.2 p.p.m. for continental, 'noisy' sites (Fig. 2).

The 11 land basis region boundaries were constructed to enclose vegetation of similar seasonal structure and carbon exchange based on vegetation classification[21]. Ocean basis regions were chosen to approximate circulation features such as gyres and upwelling regions. Unit emissions of 1 Gt C yr^{-1} were specified from each region. Subregional-scale variations in emissions rates were prescribed for land regions according to simulated net primary production from the CASA model[21]. This assumes that carbon fluxes follow the distribution of vegetation productivity. Emissions from ocean regions were prescribed as spatially uniform, except that sea-ice was masked out using seasonally varying fractional ice cover distributions[22]. The inversion requires prior flux and uncertainty estimates. Our choices have been guided by ocean and terrestrial flux models and observations[10,19], and are shown in Fig. 1 (also see Table 2 in Supplementary Information). The land region prior flux estimates incorporate recent inventory estimates[23–30]. Where more than one estimate for a given region was considered, a mid-point of the estimate spread was used. The prior flux uncertainty was chosen to be large enough to encompass all estimates. Prior flux uncertainties reflect one standard deviation.

The inversion is run separately for 16 transport models or model variants. The models used (and the initials of the modellers) are CSU general circulation model (K.R.G., A.S.D.), Goddard Institute for Space Studies off-line model—UCB (I.Y.F., J.J.), UCI-CTM with GISS-II' fields (M.P., B.C.P., 3 model variants), Japan Meteorological Agency—CDTM (T.M.), MATCH/CCM3 winds (L.B.), MATCH/NCEP winds (Y.H.C.), MATCH/MACCM2 winds (R.M.L.), NIES (S.M.), National Institute for Resources and Environment (S.T.), Recherche en Prevision Numerique (C.W.Y.), SKYHI (S.F.), TM2 (P.B., P.C., P.P.), TM3 (M.H.), GCTM (D.B.). The inversion produces estimated fluxes and their uncertainties for each region individually and for some groups of regions in addition to a background concentration. Here our analysis focuses on fluxes and uncertainties that are averaged across models. We also specify two measures of uncertainty as described in the main text. We show the 'between' model uncertainty as a one standard deviation confidence interval for meaningful comparison with the within model uncertainty. The obvious alternative, showing a full range, would also produce a confidence interval that would widen as more models were included. Inspection of the individual flux estimates showed them to be close to normally distributed about the mean flux for most regions.

Received 14 June; accepted 11 December 2001.

1. Enting, I. G., Trudinger, C. M. & Francey, R. J. A synthesis inversion of the concentration and $\delta^{13}C$ of atmospheric CO_2. *Tellus B* **47,** 35–52 (1995).
2. Fan, S. *et al.* A large terrestrial carbon sink in North America implied by atmospheric and oceanic carbon dioxide data and models. *Science* **282,** 442–446 (1998).
3. Kaminski, T., Heimann, M. & Giering, R. A coarse grid three-dimensional global inverse model of the atmospheric transport, 2, inversion of the transport of CO_2 in the 1980s. *J. Geophys. Res.* **104,** 18555–18581 (1999).
4. Bousquet, P., Ciais, P., Peylin, P., Ramonet, M. & Monfrey, P. Inverse modelling of annual atmospheric CO_2 sources and sinks. Part 1: method and control inversion. *J. Geophys. Res.* **104,** 26161–26193 (1999).
5. Baker, D. F. *Sources and Sinks of Atmospheric CO_2 Estimated from Batch Least-Squares Inversions of CO_2 Concentration Measurements.* Thesis, Princeton Univ. (2001).
6. Taguchi, S. Synthesis inversion of atmospheric CO_2 using the NIRE chemical transport model. *Geophys. Monogr.* **114,** 239–254 (2000).
7. Peylin, P., Baker, D., Sarmiento, J., Ciais, P. & Bousquet, P. Influence of transport uncertainty on annual mean and seasonal inversions of atmospheric CO_2 data. *J. Geophys. Res.* (submitted).
8. Rayner, P. J., Enting, I. G., Francey, R. J. & Langenfelds, R. Reconstructing the recent carbon cycle from atmospheric CO_2, $\delta^{13}C$ and O_2/N_2 observations. *Tellus B* **51,** 213–232 (1999).
9. Bousquet, P. *et al.* Regional changes in carbon dioxide fluxes of land and ocean since 1980. *Science* **290,** 1342–1346 (2000).
10. Takahashi, T. *et al.* Global sea-air CO_2 flux based on climatological surface ocean pCO_2, and seasonal biological end temperature effects. *Deep-Sea Res. I.* (submitted).
11. Tans, P., Fung, I. & Takahashi, T. Observational constraints on the global atmospheric CO_2 budget. *Science* **247,** 1431–1438 (1990)
12. Denning, S. *et al.* Three-dimensional transport and concentration of SF_6: A model intercomparison study (Transcom 2). *Tellus B* **51,** 266–297 (1999).
13. Metzl, N., Brunet, C., Jabaud-Jan, A., Poisson, A. & Schauer, B. in *Extended Abstr. 6th Int. Carbon Dioxide Conf.* 685–688 (Organizing Committee of Sixth Carbon Dioxide Conference, Sendai, 2001).
14. Kaminski, T., Rayner, P. J., Heimann, M. & Enting, I. G. On aggregation errors in atmospheric transport inversions. *J. Geophys. Res.* **106,** 4703–4715 (2001).
15. Denning, A. S., Fung, I. Y. & Randall, D. A. Latitudinal gradient of atmospheric CO_2 due to seasonal exchange with land biota. *Nature* **376,** 240–243 (1995).
16. Tarantola, A. *Inverse Problem Theory: Methods for Data Fitting and Model Parameter Estimation* 3rd impr. (Elsevier, Amsterdam, 1998).
17. Andres, R. J., Marland, G., Fung, I. & Matthews, E. Distribution of carbon dioxide emissions from fossil fuel consumption and cement manufacture, 1950-1990. *Glob. Biogeochem. Cycles* **10,** 419–429 (1996).
18. Brenkert, A. L. Carbon dioxide emission estimates from fossil-fuel burning, hydraulic cement production, and gas flaring for 1995 on a one degree grid cell basis. ⟨http://cdiac.esd.ornl.gov/ndps/ndp058a.html⟩ (1998; accessed Oct. 1998).
19. Randerson, J. *et al.* The contribution of terrestrial sources and sinks to trends in the seasonal cycle of atmospheric carbon dioxide. *Glob. Biogeochem. Cycles* **11,** 535–560 (1997).
20. *GLOBALVIEW-CO2: Cooperative Atmospheric Data Integration Project - Carbon Dioxide* CD-ROM (NOAA CMDL, Boulder, Colorado, 2000); also available at ⟨ftp://ftp.cmdl.noaa.gov/ccg/co2/GLOBALVIEW⟩ (2000).
21. De Fries, R. S. & Townshend, J. R. G. NDVI-derived land cover classifications at a global scale. *Int. J. Remote Sensing* **15,** 3567–3586 (1994).
22. Taylor, K. E., Williamson, D. & Zwiers, F. AMIP II sea surface temperature and sea ice concentration boundary conditions. ⟨http://www–pcmdi.llnl.gov/amip/AMIP2EXPDSN/BCS/amip2bcs.html⟩ (1997).
23. Apps, M. J. & Kurz, W. A. in *Carbon Balance on World's Forested Ecosystems: Towards a Global Assessment* (ed. Kanninen, M.) 14–39 (Publications of the Academy of Finland, Helsinki, 1994).
24. Kurz, W. A. & Apps, M. J. A 70 year retrospective analysis of carbon fluxes in the Canadian forest sector. *Ecol. Applicat.* **9,** 526–547 (1999).
25. *Greenhouse Gas Inventory Data from 1990 to 1998* (Secretariat of the United Nations Framework Convention on Climate Change, National Communications from Parties Included in Annex 1 to the Convention, FCCC/SBI/2000/11, Bonn, 2000).
26. Pacala, S. *et al.* Convergence of land- and atmosphere-based U.S. carbon sink estimates. *Science* **292,** 2316–2320 (2001).
27. Houghton, R. A. The annual net flux of carbon to the atmosphere from changes in land use 1850-1990. *Tellus B* **51,** 298–313 (1999).
28. Dixon, R. K. *et al.* Carbon pools and flux of global forest ecosystems. *Science* **263,** 185–190 (1990).

© 2002 Macmillan Magazines Ltd

29. Houghton, R. A. & Hackler, J. L. Emissions of carbon from forestry and land-use change in tropical Asia. *Glob. Change Biol.* **5,** 481–492 (1999).
30. Kauppi, P. E., Mielikainen, K. & Kuusela, K. Biomass and carbon budget of European forests, 1971 to 1990. *Science* **256,** 70–74 (1992).

Supplementary Information accompanies the paper on *Nature*'s website (http://www.nature.com).

Acknowledgements

We thank B. Stephens for comments and suggestions on earlier versions of the manuscript. This work was supported by the NSF, NOAA and the International Geosphere Biosphere Program/Global Analysis, Interpretation, and Modeling Project. S.F. and J.S. were supported by NOAA's Office of Global Programs for the Carbon Modeling Consortium.

Correspondence and requests for materials should be addressed to A.S.D. (e-mail: denning@atmos.colostate.edu).

Unsuspected diversity among marine aerobic anoxygenic phototrophs

Oded Béjà*†, Marcelino T. Suzuki*, John F. Heidelberg‡, William C. Nelson‡, Christina M. Preston*, Tohru Hamada§†, Jonathan A. Eisen‡, Claire M. Fraser‡ & Edward F. DeLong*

** Monterey Bay Aquarium Research Institute, Moss Landing, California 95039-0628, USA*
‡ The Institute for Genomic Research, Rockville, Maryland 20850, USA
§ Marine Biotechnology Institute, Kamaishi Laboratories, Kamaishi City, Iwate 026-0001, Japan

Aerobic, anoxygenic, phototrophic bacteria containing bacteriochlorophyll *a* (Bchl*a*) require oxygen for both growth and Bchl*a* synthesis[1–6]. Recent reports suggest that these bacteria are widely distributed in marine plankton, and that they may account for up to 5% of surface ocean photosynthetic electron transport[7] and 11% of the total microbial community[8]. Known planktonic anoxygenic phototrophs belong to only a few restricted groups within the Proteobacteria α-subclass. Here we report genomic analyses of the photosynthetic gene content and operon organization in naturally occurring marine bacteria. These photosynthetic gene clusters included some that most closely resembled those of Proteobacteria from the β-subclass, which have never before been observed in marine environments. Furthermore, these photosynthetic genes were broadly distributed in marine plankton, and actively expressed in neritic bacterioplankton assemblages, indicating that the newly identified phototrophs were photosynthetically competent. Our data demonstrate that planktonic bacterial assemblages are not simply composed of one uniform, widespread class of anoxygenic phototrophs, as previously proposed[8]; rather, these assemblages contain multiple, distantly related, photosynthetically active bacterial groups, including some unrelated to known and cultivated types.

Most of the genes required for the formation of bacteriochlorophyll-containing photosystems in aerobic, anoxygenic, phototrophic (AAP) bacteria are clustered in a contiguous, 45-kilobase (kb) chromosomal region (superoperon)[6]. These include *bch* and *crt* genes coding for the enzymes of the bacteriochlorophyll and carotenoid biosynthetic pathways, and the *puf* genes coding for the subunits of the light-harvesting complex (*pufB* and *pufA*) and the reaction centre complex (*pufL* and *pufM*). To better describe the nature and diversity of planktonic, anoxygenic, photosynthetic bacteria, we screened a surface-water bacterial artificial chromo-

† Present addresses: Department of Biology, Technion-Israel Institute of Technology, Haifa 32000, Israel (O.B.); Nara Institute of Science and Technology, Takayama, Ikoma 630-0101, Japan (T.H.).

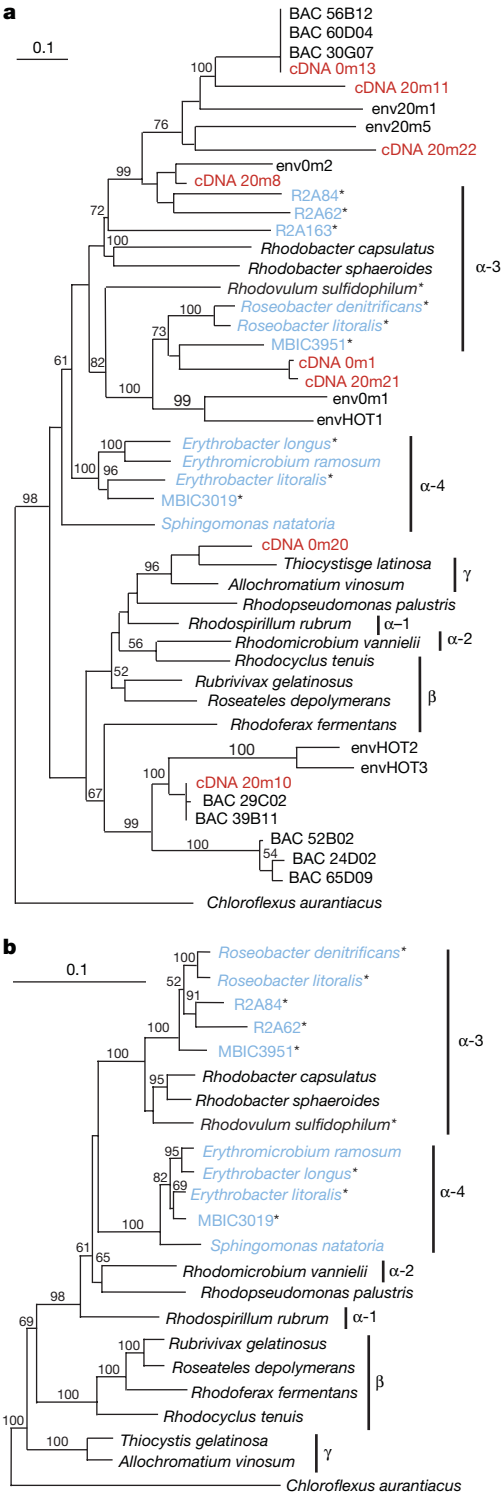

Figure 1 Phylogenetic relationships of *pufM* gene (**a**) and rRNA (**b**) sequences of AAP bacteria. **a**, **b**, Evolutionary distances for the *pufM* genes (**a**) were determined from an alignment of 600 nucleotide positions, and for rRNA genes (**b**) from an alignment of 860 nucleotide sequence positions. Evolutionary relationships were determined by neighbour-joining analysis (see Methods). The green non-sulphur bacterium *Chloroflexus aurantiacus* was used as an outgroup. *pufM* genes that were amplified by PCR in this study are indicated by the env prefix, with 'm' indicating Monterey, and HOT indicating Hawaii ocean time series. Cultivated aerobes are marked in light blue, bacteria cultured from sea water are marked with an asterisk, and environmental cDNAs are marked in red. Photosynthetic α-, β- and γ-proteobacterial groups are indicated by the vertical bars to the right of the tree. Bootstrap values greater than 50% are indicated above the branches. The scale bar represents number of substitutions per site.

© 2002 Macmillan Magazines Ltd